



ORIGINAL ARTICLE

Honey-mediated synthesis of Cr₂O₃ nanoparticles and their potent anti-bacterial, anti-oxidant and anti-inflammatory activities



Hamna Shahid ^a, Iqra Arooj ^{a,*}, Saba Zafar ^b, Saba ^a

^a Department of Microbiology & Molecular Genetics, Faculty of Life Sciences, The Women University, Multan 66000, Pakistan

^b Institute of Biochemistry & Biotechnology, Faculty of Life Sciences, The Women University, Multan 66000, Pakistan

Received 18 October 2022; accepted 2 January 2023

Available online 5 January 2023

KEYWORDS

Chromium oxide;
K. pneumoniae;
Nanoparticles;
Honey

Abstract Green synthesis of nanoparticles has gained tremendous attention in recent era which is pertinent to their unique properties and broad applications. This approach is cost-effective, environment-friendly as well as highly biocompatible. In this research, chromium oxide nanoparticles (Cr₂O₃-NPs) were synthesized by using *Apis mellifera* honey as a reducing and capping agent and their anti-bacterial, anti-biofilm, anti-oxidant and anti-inflammatory abilities were explored. Ultra Violet-visible double beam spectroscopy revealed that chromium underwent d-d transition during synthesis of nanoparticles. X-ray diffraction (XRD) analysis verified that Cr₂O₃-NPs were crystalline in nature and average crystal size was 24 nm. Energy-dispersive X-ray (EDX) analysis confirmed that chromium and oxygen formed nano-composites in solution which possessed a stable form. Scanning electron microscopy (SEM) provided morphological characteristics of nanoparticles and proved that their average size was 20 nm. Cr₂O₃-NPs displayed excellent anti-bacterial activity (minimum inhibition zone, 20 mm; maximum inhibition zone, 26 mm) against 30 selected clinical isolates of *Klebsiella pneumoniae* as determined by agar well-diffusion method. Their antibacterial activity was considerably superior to that of three selected antibiotics including Gentamicin, Ciprofloxacin and Cefepime. However, no synergism was observed between nanoparticles and these antibiotics as calculated from fractional inhibitory concentration index (FICI) values all of which were > 1. The synthesized nanoparticles possessed good biofilm inhibition potential (60 % to 73 %) at all concentrations (20 µg/ml to 50 µg/ml) tested. Cr₂O₃-NPs exhibited excellent anti-oxidant activity (IC₅₀ = 128 µg/ml) which was nearly equivalent to that of ascorbic acid. Anti-inflammatory effect of Cr₂O₃-NPs was also significant (IC₅₀ = 549 µg/ml) and comparable to that of standard. Both anti-oxidant and anti-inflammatory capacities were found to increase with an

* Corresponding author at: Department of Microbiology & Molecular Genetics, The Women University, Multan, Pakistan.

E-mail address: iqra.6051@wum.edu.pk (I. Arooj).

Peer review under responsibility of King Saud University.



increase in the concentration of Cr₂O₃-NPs. In conclusion, this work revealed that *Apis mellifera* honey-mediated synthesis of Cr₂O₃-NPs could be investigated for future biomedical applications.

© 2023 The Author(s). Published by Elsevier B.V. on behalf of King Saud University. This is an open access article under the CC BY-NC-ND license (<http://creativecommons.org/licenses/by-nc-nd/4.0/>).

1. Introduction

Antibiotic resistance has become a global health issue as microorganisms can quickly adapt to the changing environments and gain resistance to the available antibiotics (Chokshi et al., 2019). One of the solutions proposed in this regard is utilization of therapeutic nanoparticles, particularly the metallic ones. Metallic nanomaterials draw together a variety of disciplines including nanomedicine, drug delivery as well as chemical and green engineering to fight antibiotic resistance in multi-drug resistant bacteria (Das and Pradhan, 2022). The widespread use of nanotechnology in different fields, especially nanomedicine, has energized nanoparticles synthesis (Rasouli et al., 2018). There are numerous strategies for producing metallic nanoparticles although, in view of stability, cost-effectiveness, and environmental impacts, the green synthesis approach is preferable (Olga et al., 2022).

Klebsiella pneumoniae is emerging as a bacterial pathogen that can potentially cause life-threatening illness. The ability of *K. pneumoniae* to modify its genetic material is a crucial attribute that has contributed towards its pathogenicity and multi-drug resistance (Russo and Marr, 2019). In both immunosuppressed and immunologically normal patients, *K. pneumoniae* is notorious for causing nosocomial infections. Various strains of *K. pneumoniae* have gained resistance to carbapenem antimicrobials and are considered a pivotal problem by World Health Organization (WHO) (Choby et al., 2020). Previously, several metals and metal oxides, including gold, silver, platinum, copper oxide, zinc oxide, cerium oxide and many others have been useful in biological synthesis approaches employing plants as well as microorganisms (Kalaycıoğlu et al., 2022). Among these, chromium oxide (Cr₂O₃) has gained the interest of researchers because of its reliability, melting point (2,300 °C), and energy band gap of 3.4 eV (Iqbal et al., 2020). Furthermore, Cr₂O₃ nanoparticles (Cr₂O₃-NPs) are remarkable inorganic materials with excellent properties for a variety of contemporary science and technology fields. Biomedical strategies to manufacture Cr₂O₃-NPs from plants and organic biomass have been deemed appropriate because of their ecologic, financial, and pharmacological benefits. Green synthesized Cr₂O₃ nanomaterials have expanded their implementations as microbicial, fungicidal, anti-carcinogenic, and anti-leishmanial agents (Ghotekar et al., 2021; Nivethitha and Rachel, 2020). In the recent years, many oxides of chromium have been reported such as Cr₃O₈, Cr₅O₁₂, Cr₂O₅, and Cr₆O₁₃. However, among these different oxides, trivalent oxide (Cr₂O₃) is identified as a stable one (Sone, et al., 2016).

Biogenic synthesis of nanomaterials confers several distinct characteristics such as formfitting size, homogeneous shape, excellent scattering, exemplary physical and thermal stability, high surface hydrophilicity, and the capacity to further modify the surface (Wang et al., 2022). In previous years, Cr₂O₃-NPs were prepared by using different plants including *Callistemon viminalis* and *Rhamnus virgata* as well as natural honey (Sone et al., 2016, Iqbal et al., 2020, Nivethitha and Rachel, 2020). Among these, natural honey has always been considered as an ancient source of food with unrivalled medicinal, physiological and therapeutic properties (Nivethitha and Rachel, 2020). Its unique biochemical qualities enable it to be used in the green creation of nano compositions. It contains various phytochemicals, proteins, and carbohydrates that act as reducing and stabilizing agents in the synthesis of nanoparticles (Balasooriya et al., 2017). In the past years, research of antibacterial and anti-biofilm potential of honey-mediated Cr₂O₃-NPs against clinical strains of *K. pneumoniae* has not been performed to the best of our knowledge. Hence, in the present study, Cr₂O₃-NPs were synthesized from potassium dichromate

utilizing *Apis mellifera* honey as a reducing and stabilizing agent, subsequent to which their antibacterial and antibiofilm potential was evaluated against *K. pneumoniae*. In addition, their antioxidant and anti-inflammatory activities were evaluated. It was anticipated that the production of honey-mediated chromium oxide nanomaterials may prove to be a simple, cost-effective, coherent, rapid, and secure alternative to existing antibacterial drugs.

2. Materials & methods

2.1. Honey-mediated synthesis of chromium oxide nanoparticles

Organic honey produced from *Apis mellifera* was purchased from the local market of Multan, Pakistan and stored at room temperature for future use. Cr₂O₃-NPs were synthesized from the reduction of potassium dichromate by utilizing 20 % honey solution. For this, 5 g of K₂Cr₂O₇ was diluted in 50 ml of distilled water and stirred well. 20 ml of honey was then added drop-by-drop to the prepared bright orange solution of K₂Cr₂O₇. At first, the solution was heated at 60 °C for approximately 20 min and then stirred vigorously to get dark green color. The final solution was cooled down, washed with distilled water, and filtered by using Whatman filter paper. Fine powder of solution was made by keeping the solution in hot air oven at 80 °C for the next 18–20 h.

2.2. Characterization of chromium oxide nanoparticles

Various analysis methods were used to characterize the biogenic chromium nanomaterials. Spectral absorbance of Cr₂O₃-NPs was measured in the range of 200–600 nm by using the UV–visible spectrophotometer for primary confirmation. Crystallographic structure of Cr₂O₃-NPs was evaluated through X-ray Diffractometer (Bruker D8 Discover). Powdered sample was kept in the diffractometer under 50–500 μm X-ray beam, which revealed the point analysis of specific areas in the sample (usually size is in μm). Elemental composition of Cr₂O₃-NPs was determined by using EDAX Team (EDX/SEM). The instrument was set at 12.5 kV, 3.84 A, 500 X, and 129 eV. Three different spots were analyzed under these specific conditions, which further revealed the presence of elements in each specific area. Size and morphological characteristics of Cr₂O₃-NPs were observed under the scanning electron microscope (Emcraft) with potential energy of 2.1 kV, and magnification from 40 to 2000 X, specifically.

2.3. Antibacterial activity of nanoparticles

The agar well-diffusion method was used to record the antibacterial potential of synthesized nanoparticles against the clinical isolates of *K. pneumoniae*. A total of 30 clinical isolates of *K. pneumoniae* were obtained from Microbiology laboratory of Nishter Hospital, Multan, Pakistan between October and December, 2021. Sterilized MH-agar plates were

prepared and each plate was swabbed with 0.5 McFarland standard bacterial culture. After 20 min of drying, three wells of approximately equal size were fabricated at equal distance with the help of pasteur pipettes on each plate. First two wells were filled with 30 μ l of Cr₂O₃-NPs and the third well was filled with 30 μ l of raw honey solution. Deionized water was included as a negative control in the experiment. MH-agar plates were incubated at 37° C overnight. Diameter of inhibition zones was measured in millimeters for each isolated strain afterwards (Maheo et al., 2022). Minimum inhibitory concentration (MIC) of Cr₂O₃-NPs against *K. pneumoniae* was performed in a 96-well plate with the help of standard broth dilution method. Various concentrations of nanoparticles (20–50 μ g/ml) in LB broth were made. Approximately, 180 μ l of 20–50 μ g/ml Cr₂O₃-NPs suspension was added in each of the wells. 20 μ l of 0.5 McFarland standard bacterial culture was mixed with dilutions in the wells and incubated at 37° C overnight. The experiment was performed in triplicates and results were determined by using microtiter plate reader (OD₆₂₀ nm) (Perveen et al., 2022).

2.4. Synergistic activity of Cr₂O₃-NPs with selected antibiotics

Gentamicin (CN-10), Ciprofloxacin (CIP-5) and Cefepime (FEP-30) were selected to test the synergism with synthesized nanoparticles. Firstly, antibiotic susceptibility testing was performed against each clinical strain of *K. pneumoniae* using antibiotics alone. Results were summarized according to the CLSI guidelines. Next, well-diffusion method was used to record the synergistic potential of Cr₂O₃-NPs with selected antibiotics against each clinical strain. Bacterial lawns were made on each MH-plate. Three wells of appropriate size were made with the help of pasteur pipette. In each well, only one antibiotic was placed and wells were filled with 30 μ l of synthesized nanoparticles. Plates were placed in incubator at 37 °C and the very next day, plates were examined for synergistic activity. Zones of inhibition were measured and recorded in millimeters. For synergism, fractional inhibitory concentration index (FICI) values (0.5 or \leq 1) were calculated by using the following formula:

$$FICI = \frac{NPs' antibacterialeffect + Antibiotic's antibacterialeffect}{Antibacterialeffectofboth}$$

2.5. Anti-biofilm potential of Cr₂O₃-NPs

Sterile 96-well plates were used to determine the anti-biofilm potential of Cr₂O₃-NPs. Various concentrations of nanoparticles (20–50 μ g/ml) in LB broth were made. Biofilms of *K. pneumoniae* were grown on the plates by inoculating each well with 20 μ l of standardized bacterial culture (OD₆₀₀ = 0.3). After 72 h of incubation, approximately, 180 μ l of 20–50 μ g/ml dilutions (Cr₂O₃-NPs + broth) was added in the wells of plates. Plates were incubated for the next 18 h. Biofilms were washed with PBS twice or thrice by discarding media and unwanted bacterial suspension. After 20 min of drying, biofilms were stained with crystal violet solution. Plates were allowed to sustain stain at room temperature for 20–25 min and after that, unreacted stain was removed with 90 % ethanol solution. Biofilms without nanoparticles were considered as positive control in this protocol. The experiment was performed in triplicates

and results were measured by using microtiter plate reader (OD₆₂₀ nm) (AlSalhi et al., 2022).

$$Biofilminhibition(\%) = (OD_{control} - OD_{sample}) / OD_{control} \times 100$$

2.6. Antioxidant potential of Cr₂O₃-NPs

Antioxidant potential of Cr₂O₃-NPs was calculated by performing phosphomolybdenum spectrophotometric method. Working solution consisting of 4 mM ammonium molybdate, 0.6 M sulfuric acid, and 28 mM sodium phosphate as well as various aqueous concentrations (200–800 μ g/ml) of nanoparticles were utilized for this purpose. 1 ml of working solution was mixed with 100 μ l of each of the aqueous concentrations of nanoparticles in different test tubes. Test tubes were then incubated at 95 °C in water bath for 90 minutes. After incubation period, test tubes were allowed to cool down at room temperature. In this experiment, ascorbic acid was used as control. Absorbance of each solution was measured by using spectrophotometer at 695 nm. Total antioxidant capacity (TAC) as percentage was calculated by using the following formula:

$$Totalantioxidantcapacity(\%) = (OD_{control} - OD_{sample}) / OD_{control} \times 100$$

The procedure was repeated three times, and the outcomes were summed up by determining half-maximal inhibitory concentration (IC₅₀) value (Nivethitha & Rachel, 2020).

2.7. Anti-inflammatory potential of Cr₂O₃-NPs

Working solution (0.2 % w/v) of bovine serum albumin (BSA) and various aqueous concentrations (200–800 μ g/ml) of nanoparticles were used to explore anti-inflammatory activity of synthesized nanoparticles. 5 ml of BSA solution was mixed with aqueous suspension of nanoparticles at different concentrations in separate test tubes. Test tubes were then incubated at 75 °C in water bath for five minutes. After incubation period, test tubes were allowed to cool down at room temperature. In this experiment, ascorbic acid was used as control. Absorbance of each solution was measured at 660 nm. Anti-inflammatory capacity was estimated by using the following formula:

$$Anti - inflammatorycapacity(\%) = (OD_{control} - OD_{sample}) / OD_{control} \times 100$$

The procedure was repeated three times and the average results were summed up by determining half-maximal inhibitory concentration (IC₅₀) value (Vernekar and Taranath, 2022).

3. Results

3.1. Honey-mediated synthesis of chromium oxide nanoparticles

The nanoparticle formation began when honey was mixed with potassium dichromate solution and heated. Development of emerald (dark green) color gave visual prediction of the presence of nanoparticles in solution (Fig. 1). Further confirmation was done based on spectroscopic analysis where two high-

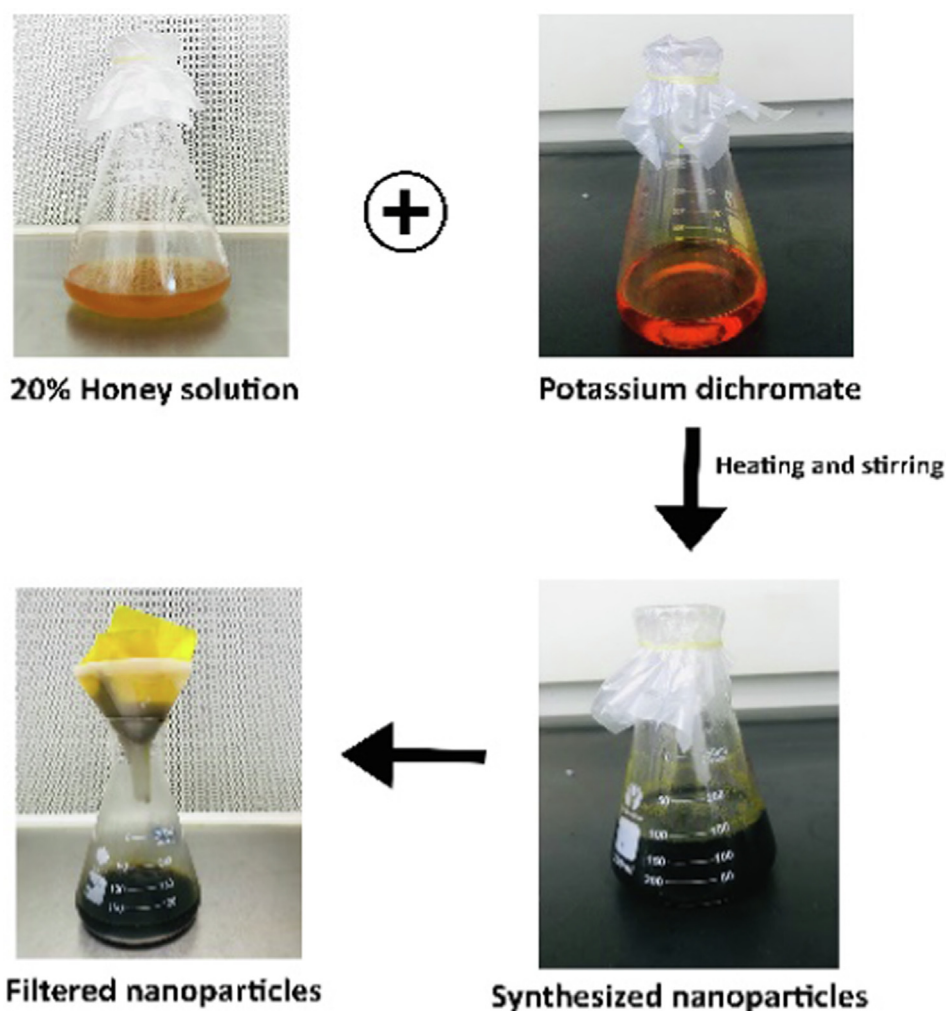


Fig. 1 Color change in reaction mixture provided visual indication for synthesis of Cr_2O_3 -NPs.

intensity peaks were observed at around 365 nm and 450 nm, respectively (Fig. 2). The peak between 400 and 450 nm is attributed to d-d transition of metal during the process of synthesis.

3.2. Characterization of chromium oxide nanoparticles

XRD analysis shown in Fig. 3a displays Bragg's diffraction peaks at $2(\theta) = 24.3, 32.4, 35.6, 38.7, 42.0, 44.9, 50.3$ and 52.4 with miller index values or planes of (012), (104), (110), (006), (113), (202), (024) and (116), respectively. These crystal planes indicated that synthesized Cr_2O_3 -NPs were crystalline in nature. Average size of crystal was calculated as 24 nm. EDX analysis revealed the surface chemical composition of fabricated nanoparticles (Fig. 3b). Clear illustrations of different peaks of elements present in the sample were obtained. The high intensity K- α peak of Cr and O between 0.0 and 0.83 keV confirmed the presence of chromium and oxygen in formed nano compositions. It showed that crystalline nanoparticles of chromium oxide were the most abundantly present specie in the sample. However, potassium was also present and various ionic fractions represented a minute part of the sample. Results of SEM analysis have been

illustrated in Fig. 3c and they depicted the morphological characteristics of manufactured nanomaterials. Synthesized nanoparticles were arranged in irregular rocky clusters and 20–30 nm average size was estimated for them at 2000X magnification.

3.3. Antibacterial potential of nanoparticles

Synthesized nanoparticles showed significant in vitro antibacterial efficacy against all isolated strains of *K. pneumoniae* at a concentration of $30 \mu\text{g/ml}$ (Fig. 4a). However, honey alone did not show any significant bactericidal potential (Fig. 4b). Maximum inhibition zones of 26 mm against HS-K-1, HS-K-2, HS-K-9, and minimum inhibition zones of 20 mm against HS-K-7, HS-K-20, HS-K-22, HS-K-28 were elucidated for the synthesized nanoparticles. Intermediate values were recorded against the remaining bacterial isolates. A zone diameter of 21 mm was measured against HS-K-4, HS-K-8, HS-K-12, HS-K-14, HS-K-15, HS-K-16, HS-K-17, HS-K-19 as well as HS-K-27. In addition, inhibition zones of 22 mm were measured against HS-K-3, HS-K-5, HS-K-6, HS-K-10, HS-K-11, HS-K-13, HS-K-21, HS-K-24, HS-K-26 and HS-K-30. Finally, inhibition zones measuring 23 mm and 24 mm were

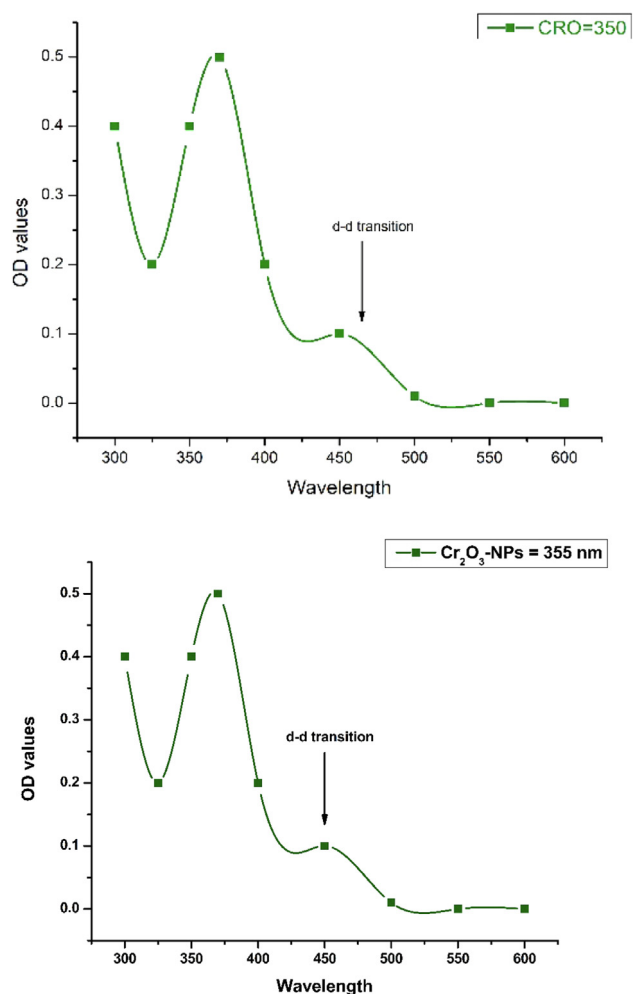


Fig. 2 UV-Visible spectroscopic analysis of Cr₂O₃-NPs.

recorded against HS-K-18, and HS-K-23, respectively, while those measuring 25 mm were demonstrated against HS-K-25 and HS-K-29. 20 µg/ml was interpreted as minimal inhibitory concentration for fabricated nanoparticles against *K. pneumoniae* based on optical density values obtained from microtiter plate reader.

3.4. Synergistic activity of Cr₂O₃-NPs with selected antibiotics

When antibiotics were used alone, it was revealed that all of the *K. pneumoniae* strains were intermediate resistant to CN-10 and FEP-30 while all strains were susceptible to CIP-5. Fig. 5 illustrates the comparison of synergistic antibacterial activity with that of crude Cr₂O₃-NPs and antibiotics alone. It can be clearly observed that, in most instances, nanoparticles alone demonstrated the highest antibacterial activity when compared with antibiotics and combination of nanoparticles and antibiotics. Antibiotics proved to be the least effective of all at most of the occasions. In majority of the cases, antibacterial activity of nanoparticles decreased when they were combined with antibiotics which emphasizes that synthesized Cr₂O₃-NPs didn't show synergistic activity with any antibiotic. FICI values calculated for these strains were also greater than 1 (1.75, 1.5, 1.7, 1.8, 1.6, 1.75, 1.8), further highlighting the lack of synergism.

3.5. Anti-biofilm potential of Cr₂O₃-NPs

The findings from quantitative anti-biofilm activity assay revealed that Cr₂O₃-NPs displayed good biofilm inhibition potential at all concentrations used for analysis. It was indicated that even the lowest (20 µg/ml) concentration of NPs showed 60 % anti-biofilm activity. Other concentrations including 30 µg/ml, 40 µg/ml, and 50 µg/ml of synthesized nanoparticles presented 64 %, 68 %, and 73 % biofilm inhibition, respectively (Fig. 6a).

3.6. Antioxidant potential of Cr₂O₃-NPs

Different concentrations of manufactured nanoparticles showed excellent antioxidant potential when compared to ascorbic acid (AAE). 0.96, 1.15, 2.06, and 2.3 absorbance values were measured for Cr₂O₃-NPs while 2.48, 2.5, 2.68, and 2.71 absorbance values were measured for AAE at 200 µg/ml, 400 µg/ml, 600 µg/ml, and 800 µg/ml concentrations, respectively. For honey, 2.15, 2.25, 2.34 and 2.46 absorbance values were measured at the same concentrations, correspondingly. 128 µg/ml was calculated as IC₅₀ value for Cr₂O₃-NPs in terms of their antioxidant efficacy (Fig. 6b). Noteworthy antioxidant potential of Cr₂O₃-NPs was observed as demonstrated in Fig. 6c, which is approximately equivalent to ascorbic acid. It was also deduced from optical density values that antioxidant activity increased with an increase in the nanoparticles' concentration in the sample.

3.7. Anti-inflammatory potential of Cr₂O₃-NPs

All concentrations (200–600 µg/ml) of produced nanoparticles revealed good anti-inflammatory potential when compared to standard, ascorbic acid. 0.66, 0.71, and 0.85 absorbance values were measured for Cr₂O₃-NPs while 2.48, 2.50, and 2.68 absorbance values were measured for AAE at 200 µg/ml, 400 µg/ml, and 600 µg/ml concentrations, respectively. At the same concentrations, absorbance values of 2.15, 2.25 and 2.34 were measured for honey. An IC₅₀ value of 549 µg/ml was estimated for synthesized nanoparticles in terms of their anti-inflammation potential (Fig. 6b). Absorbance values included in Fig. 6d demonstrate that as concentration of nanoparticles increased, their anti-inflammatory effect also increased.

4. Discussion

Chromium oxide nanomaterials were successfully synthesized by utilizing pure and local honey as reducing and stabilizing agent. Formation of nanomaterials was clearly detected by observing change of color to dark green after addition of chromium metal salt to honey solution. According to Nivethitha and Rachel (2020), change in color of metal salt from dark orange to dark green gave clear confirmation of Cr₂O₃-NPs synthesis. Hassan et al (2019) synthesized Cr₂O₃-NPs from *Callistemon viminalis* flower aqueous extracts and reported that final solution had black-green color. Surface plasmon resonance (SPR) effect on the nanoparticle's interface is responsible for change in color (Hassan et al., 2019; Iqbal et al., 2020; Khan et al., 2021). The slight difference in color most probably

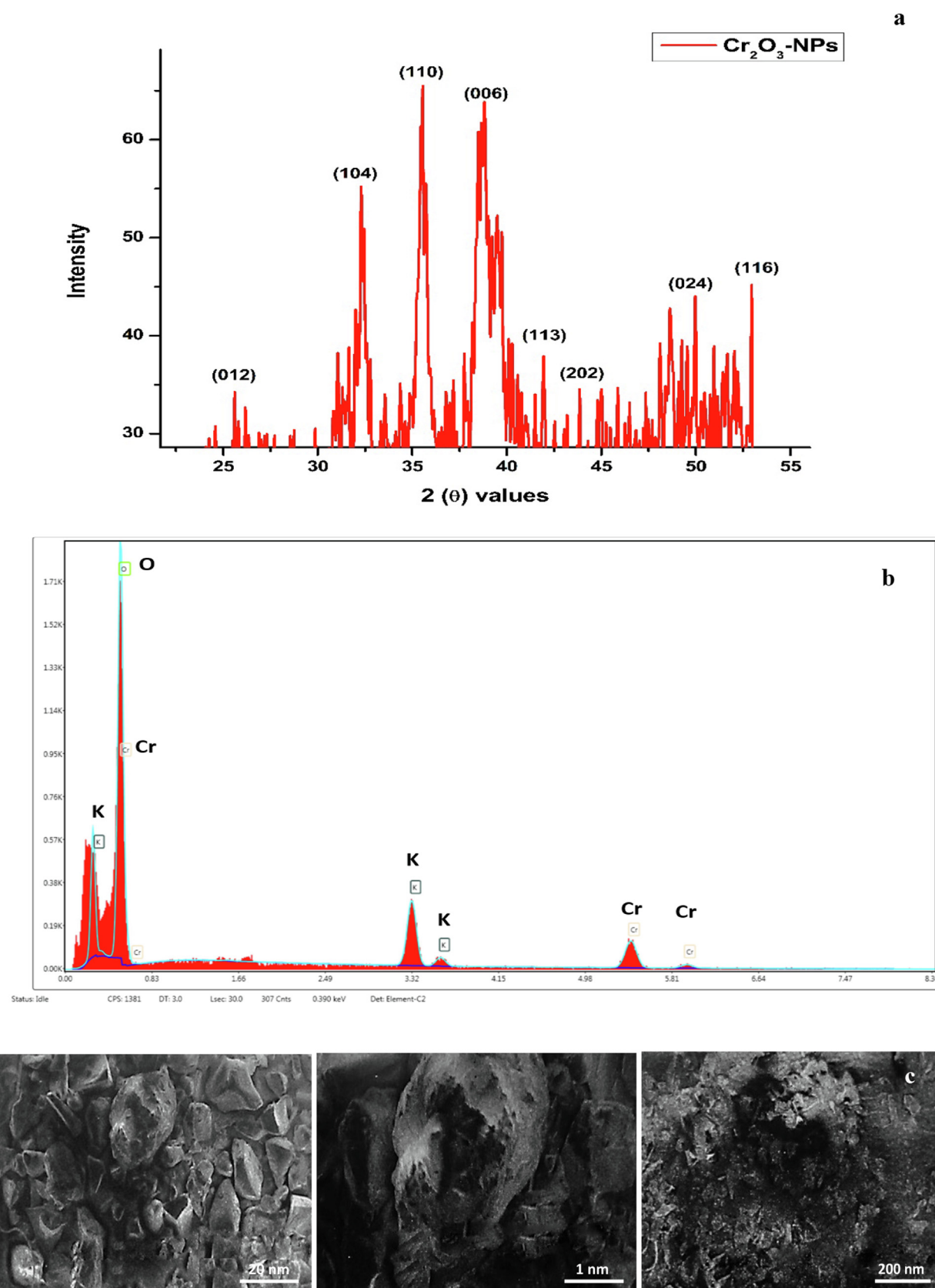


Fig. 3 Characterization of Cr_2O_3 -NPs (a) XRD analysis; (b) EDX analysis; (c) SEM images at different magnifications.

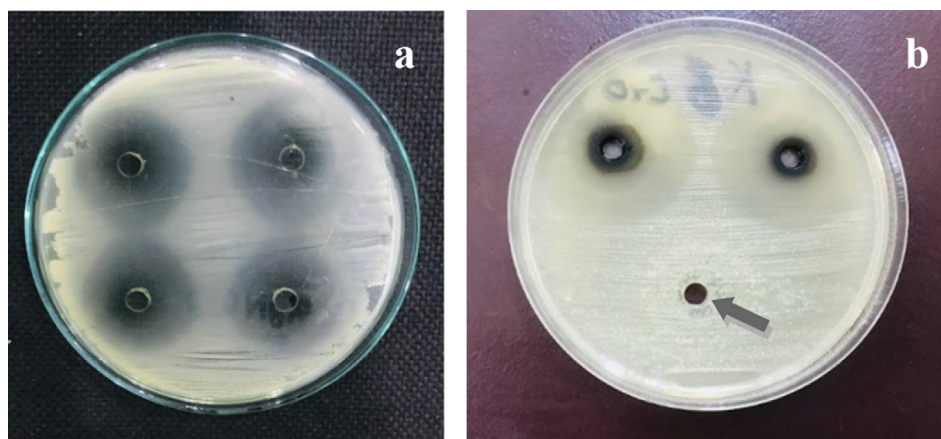


Fig. 4 MH-agar plates showing (a) strong antibacterial effect of Cr₂O₃-NPs; (b) no antibacterial effect of honey as indicated by the arrow.

depends on the green source and chromium salt used in the synthesis process.

Findings from the UV–visible spectrum showed that there were two broad absorption peaks at around 365 nm and 450 nm. Previous studies also reported two absorption peaks which correspond to Cr₂O₃-NPs. Nivethitha and Rachel (2020), Khan et al. (2021), Hassan et al. (2019), Ahmad et al (2018), Sharma and Sharma (2021), and Iqbal et al. (2020) reported strenuous peaks at 217 nm & 373 nm, 280 nm & 415 nm, 270 nm & 371 nm, 421 nm & 587 nm, 425 nm, and 269 nm & 369 nm, respectively. Although the exact values differ in each study but general SPR range of Cr₂O₃-NPs is between 250 and 450 nm. Results revealed that the SPR of Cr₂O₃-NPs is affected by the type of extract, heating, pH, and method of manufacture, which further impacts their physical attributes. The method of investigation influences crucial information about the Cr₂O₃-NPs' shape, resilience, architecture, and aggregation (Ahmed-Mohamed et al., 2020; Ghotekar et al., 2021).

XRD analysis was used to determine the crystalline nature of the synthesized nanoparticles. The intense peaks observed were compared with the Joint Committee on Powder Diffraction Standards (JCPDS). XRD graph of biogenic Cr₂O₃-NPs indicated the presence of impurities in the sample. Debye–Scherer's equation was used to calculate the average crystalline size (24 nm) of nanoparticles: $\Phi = 0.9\lambda/\beta\cos$, where β is the full-width half maximum (FWHM), λ is the X-rays wavelength and θ is the angle subtended in the peak. These observations were comparable with previous studies which yielded similar findings. (Hao et al., 2019; Iqbal et al., 2020; Ahmed-Mohamed et al., 2020; Tsegay et al., 2021).

The elemental proportions in the powdered sample were determined by EDX plots. In addition to nanoparticles which were the most abundant, impurities were also discovered in the powdered sample. Presence of impurities in solution depends, possibly, on the manufacturing method of nanoparticles. Nanostructures develop all through the solution, and residues like K and Na help to stabilize the metal-solution contact. Contaminants end up at the crystal structure created by the aggregation of these nanoparticles' internal interfaces. Although the interfaces become steadily more secure during this phase, a significant number of K atoms are still catalyti-

cally entrapped by the shifting surfaces of the developing nanocrystals. Numerous other investigations reported similar observations about the pure biogenesis of Cr₂O₃-NPs (Kim et al., 2022; Iqbal et al., 2020; Tsegay et al., 2021).

SEM images revealed that the produced nanoparticles were about 20–30 nm in size and rock-like in shape. The size distribution of produced nanoparticles was reported by Ahmed-Mohamed et al in 2020, Hao et al in 2019 and Tsegay et al in 2021 to be 25 to 38 nm, 30 nm, and 45 to 55 nm, respectively. SEM is applicable to morphological features because it provides complete information about the distinct shape and average diameter (Ghotekar et al., 2021). Different researches have reported that shapes and sizes of Cr₂O₃-NPs depend on the synthesis process (temperature, pH) and chemical composition. For instance, Patra et al (2022) revealed that two different calcination temperatures used for the synthesis of nanomaterials affected the morphological characteristics of Mn₃O₄ and MnO₂ nanoparticles.

Synthesized nanoparticles were found to have strong antibacterial effect against all clinical isolates of *K. pneumoniae*. Pure honey, however, did not show any bactericidal potential. Maximum inhibition range against *K. pneumoniae* was measured as 26 mm, which is substantial in regard to medical care. When key findings from the current study were contrasted to those from earlier investigations, strong correlations were revealed (Nivethitha and Rachel, 2020; Khan et al., 2021). Several theories have been suggested to clarify the antimicrobial effects of Cr₂O₃-NPs. For instance, it has been proved that antimicrobial activity depends on the size of Cr₂O₃-NPs. Additionally, the presence of Cr³⁺ ions may have an effect on bactericidal property. One plausible explanation is that Cr₂O₃-NPs entirely encircle the microbial surface. It is worth noting that Cr₂O₃-NPs have received more attention in cell bacteriostatic research than conventional antibiotics (Kamari et al., 2019; Wang and Shao, 2017).

All 30 clinical strains of *K. pneumoniae* were intermediate resistant to gentamicin and cefepime, while all were sensitive to ciprofloxacin. A recent study was performed on 100 clinical strains of *K. pneumoniae*. Authors investigated the vulnerability of all strains and discovered greater resistance to ciprofloxacin and intermediate resistance to gentamicin and cefepime antibiotics (Šuto et al., 2022). Combining metal oxide

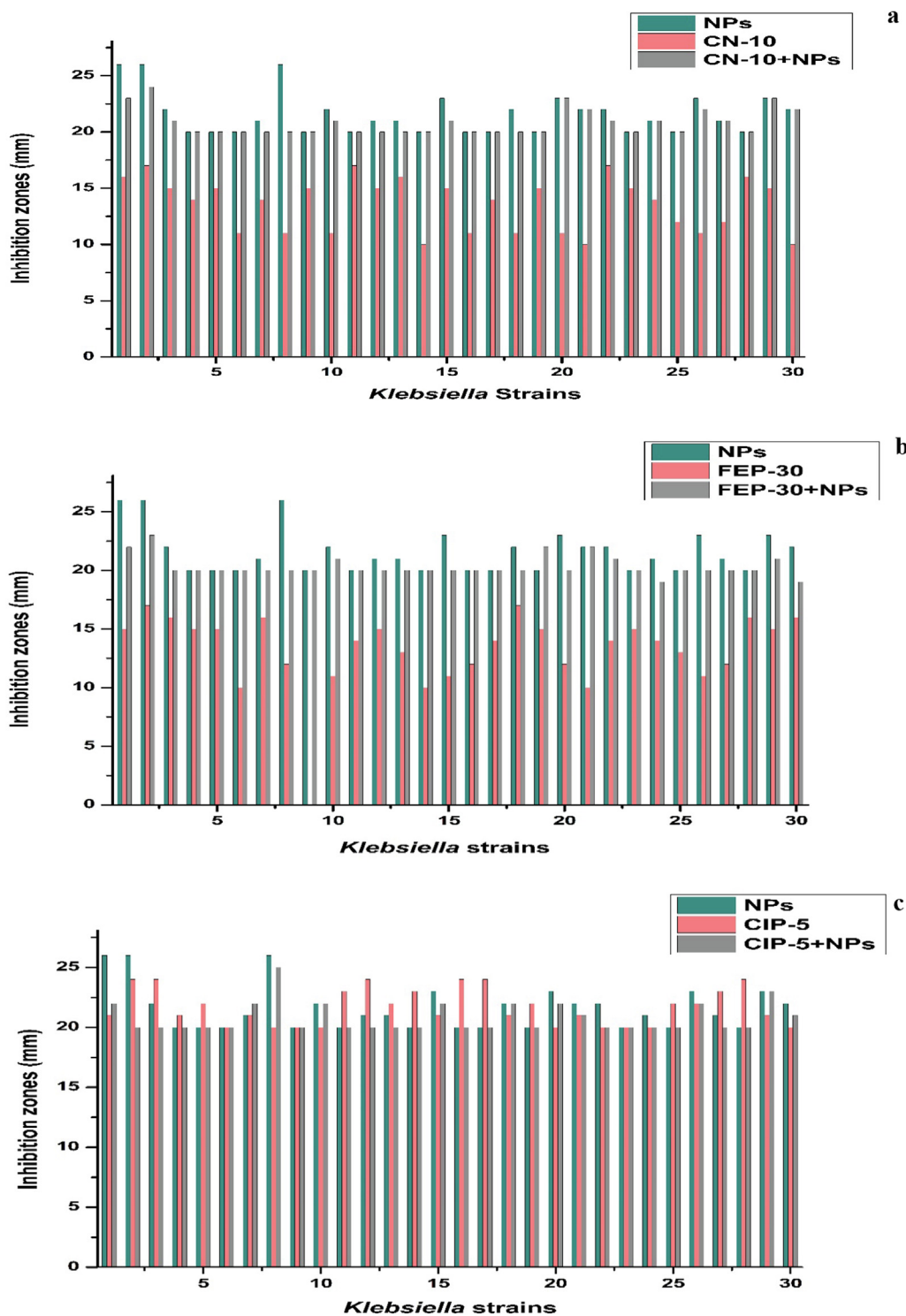


Fig. 5 Comparison of antibacterial activity of Cr_2O_3 -NPs and three different antibiotics alone with their synergistic activity against *K. pneumoniae* (a) Gentamicin (CN-10); (b) Cefepime (FEP-30); Ciprofloxacin (CIP-5).

nanoparticles with antibiotics may be useful in combating drug resistance among bacteria. Nano-science approaches can take advantage of nanomaterial-bacteria interactions to improve microbicidal effect. Antibiotics combined with tailored metal

oxide nanomaterials could thus create a brand-new class of antimicrobial drugs with enhanced synergistic effects against resistant strains (Alavi et al., 2022; Ribeiro et al., 2022). In present study, nanoparticles didn't show synergistic activity with

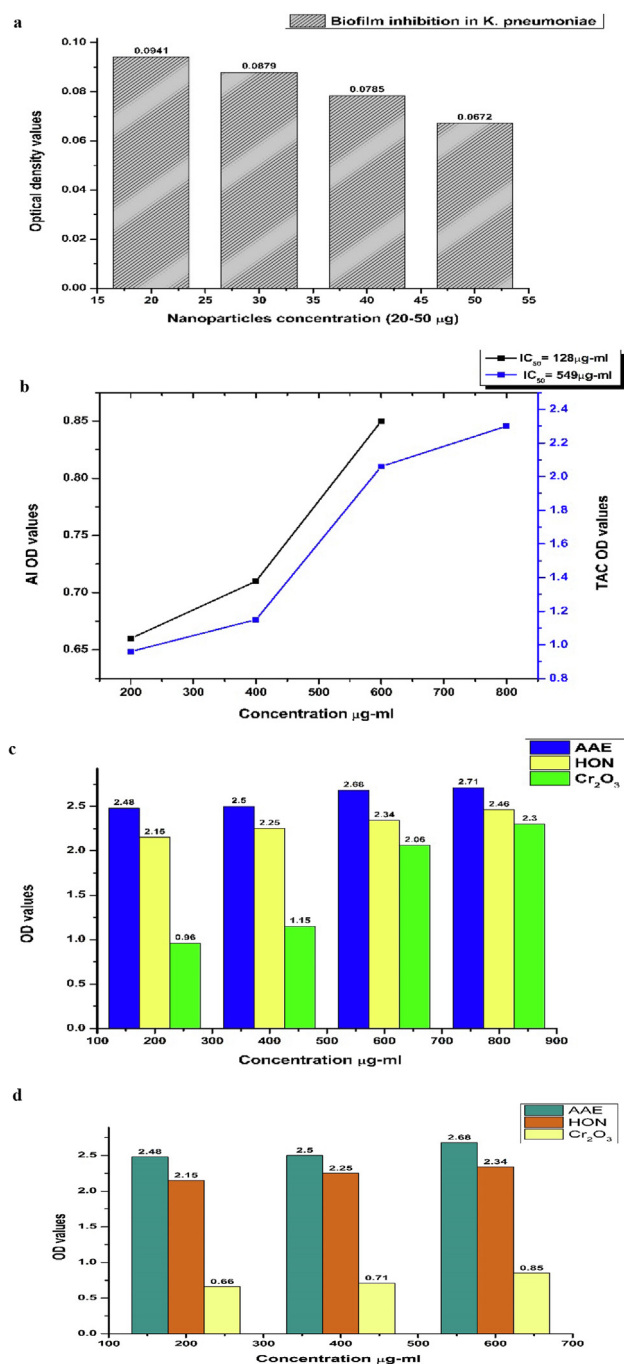


Fig. 6 (a) Biofilm inhibition potential of biogenic Cr₂O₃-NPs; (b) IC₅₀ values of Cr₂O₃-NPs for TAC and AI activity in terms of AAE. The graph clearly shows that both TAC and AI capacity of CRONPs increased with an increase in the concentration in solution; (c) Total anti-oxidant capacity of Cr₂O₃-NPs and honey in terms of AAE; (d) anti-inflammatory activity of Cr₂O₃-NPs and honey in terms of AAE.

any of the antibiotics. Additionally, it was found during the investigation that the activity of nanoparticles waned over time, resulting in older nanoparticle solutions having reduced effectiveness against the same strain. To eliminate any doubt, the synergistic effects of antibiotics and Cr₂O₃-NPs were thoroughly re-evaluated. In all experiments against every variant of *K. pneumoniae*, only one of the antimicrobial agents (antibiotic

or Cr₂O₃-NPs) was the most effective, and it was concluded that Cr₂O₃-NPs did not synergistically react with any of the drugs. Principally, only the nanoparticles showed antibacterial effect against most strains. Antibiotic combinations with NPs may or may not synergize, although this is not predictable and interactions ranging from antagonistic to > 80 % synergistic have been documented in the literature. The antibiotic class and concentration, bacterial specie, its sensitivity profile (including any resistance mechanism), and the test procedure, all affect synergism (Vardakas et al., 2019).

20 µg/ml was estimated as MIC value for synthesized Cr₂O₃-NPs. This MIC value is lower than values demonstrated in the previous studies. Al-Marjani et al (2021) demonstrated 625 µg/ml as MIC value for chemically synthesized Cr₂O₃-NPs against *K. pneumoniae*. Yassin et al (2022) estimated 10 µg/ml as MIC value for silver nanoparticles synthesized from *Origanum majorana* against *K. pneumoniae*. At 20 µg/ml, the biofilm inhibitory activity of honey-mediated Cr₂O₃-NPs was calculated to be 40 %, whereas 19 % biofilm inhibitory activity of chemically synthesized Cr₂O₃-NPs was reported at 600 µg/ml (Al-Marjani et al., 2021). Difference in MIC values is attributable to size and ROS producing potential of nanoparticles. Nanomaterials with smaller size can penetrate easily into bacteria than larger ones and they have ability to produce ROS even at their lowest concentration. Biofilm pore size is approximately 50 nm and therefore, nanomaterials with size less than 50 nm can easily penetrate the biofilms and enter the inner regions of bacteria (Sahli et al., 2022). The precise process by which Cr₂O₃-NPs destroy the biofilms was not elucidated in the present study. It was, however, observed that strains were unable to produce stable biofilms possibly, due to their less motility.

Antioxidant potential of biogenic Cr₂O₃-NPs was demonstrated in terms of ascorbic acid and significant results were recorded. The positive results were linked to the formation of dark green complex of Mo(V)-PO₄. Total antioxidant capacity was calculated by converting Mo(VI) to Mo(V) and generating a bright green Mo(V)PO₄ compound with a maximum absorbance at 695 nm (Hassan et al., 2019). The lowest concentration of NPs (200 µg/ml) gave significant TAC value (61 %) and IC₅₀ value was calculated as 128 µg/ml for Cr₂O₃-NPs. It is worth pointing out that the antioxidant potential of synthesized Cr₂O₃-NPs was only slightly lower than that of standard. Hassan et al in 2019 described the TAC value of honey mediated Cr₂O₃-NPs as 35 % at 200 µg/ml. Variation in TAC values is linked to the presence of phenolic compounds in green source from which nanoparticles were synthesized and natural extracts contain different number of phenolic compounds. Additionally, in the synthesis of Cr₂O₃, an aqueous solution of honey was used as a capping agent implying that certain phenolic substances from the honey may have capped the nanoparticles, which have the ability to quench ROS (Nivethitha and Rachel, 2020). Different studies have observed variable antioxidant capacity of other metallic nanoparticles synthesized from natural and chemical sources in relation to standard (Asghar et al., 2022; David et al., 2022; Lokapur et al., 2022; Riaz et al., 2022; Lu et al., 2021).

Anti-inflammatory activity of newly synthesized nanoparticles was determined in terms of standard and positive average results were interpreted. Positive results were linked to inhibition of BSA inflammation in the solution. The lowest concentration of newly synthesized nanoparticles (200 µg/ml)

showed AI value of 68 % and IC₅₀ value was calculated as 549 µg/ml. Results were found to be dependent on the concentration of honey used in the synthesis of nanoparticles as anti-inflammatory potential of synthesized nanoparticles is reported to be dosage-dependent. Drastic increase in the number of nanoparticles in the solution will increase anti-inflammatory effects. Rajakumar et al (2018) and Sabeena et al (2022) reported the anti-inflammatory activity of ZnO and CuO nanoparticles using BSA inhibition method and reported significant IC₅₀ values. Different studies have claimed different anti-inflammatory capacity of other metallic nanoparticles synthesized from various natural sources in terms of standard, chemically synthesized nanoparticles and aqueous extracts of green source (Chirumamilla et al., 2022; Imraish et al., 2021; Pandiyan et al., 2022; Velsankar et al., 2022; Kwak et al., 2022).

Our research was limited to the biological effect and we did not study the underlying mechanism of action of honey-mediated metal oxide nanoparticles. Few studies reported so far in this context have described that the proteins and sugars in honey are responsible for stabilization of metal oxide nanoparticles. However, more research is necessary to pinpoint the crucial components in charge for the functionalization of these metal oxide nanoparticles. It is still necessary to develop well defined protocols which produce nanoparticles from honey with narrow size distribution, so that they can be employed in drug delivery and other medical applications.

5. Conclusion

We used absolutely pure honey as a green source in the synthesis of Cr₂O₃-NPs. The formulated nanoparticles out-performed selected antibiotics in terms of their antibacterial efficacy against clinical strains of *K. pneumoniae*. The biofilm-inhibitory, anti-oxidant and anti-inflammatory effects disclosed that formulations based on Cr₂O₃-NPs synthesized from *Apis mellifera* honey can be pursued as biocompatible, biologically active, cost-effective, and environment-friendly strategy to combat antibiotic resistance in *K. pneumoniae*.

Acknowledgements

None.

Funding

None.

Conflict of Interest Statement

We declare that there is no conflict of interests regarding the publication of this article.

References

- Ahmad, Z., Shamim, A., Mahmood, S., Mahmood, T., Khan, F.U., 2018. Biological synthesis and characterization of chromium (iii) oxide nanoparticles. *Eng. Appl. Sci. Lett.* 1 (2), 23–29.
- Ahmed Mohamed, H.E., Afridi, S., Khalil, A.T., Zohra, T., Ali, M., Alam, M.M., Maaza, M., 2020. Phyto-fabricated Cr₂O₃ nanoparticle for multifunctional biomedical applications. *Nanomedicine.* 15 (17), 1653–1669.
- Al Marjani, M., Aziz, S.N., Rheima, A.M., Abbas, Z.S., 2021. Impact of chromium oxide nanoparticles on growth and biofilm formation of persistence *Klebsiella pneumoniae* isolates. *Nano Biomed. Eng.* 13 (3), 321–327.
- Alavi, M., Hamblin, M.R., Martinez, F., Kennedy, J.F., Khan, H., 2022. Synergistic combinations of metal, metal oxide, or metalloidal nanoparticles plus antibiotics against resistant and non-resistant bacteria. *Micro Nano Bio Aspects.* 1 (1), 1–9.
- AlSalhi, M.S., Devanesan, S., Rajasekar, A., Kokilaramani, S., 2022. Characterization of plants and seaweeds based corrosion inhibitors against microbially influenced corrosion in a cooling tower water environment. *Arabian Journal of Chemistry.* 104513.
- Asghar, M., Sajjad, A., Hanif, S., Ali, J.S., Ali, Z., Zia, M., 2022. Comparative analysis of synthesis, characterization, antimicrobial, antioxidant, and enzyme inhibition potential of roses petal based synthesized copper oxide nanoparticles. *Materials Chemistry and Physics.* 278, 125724.
- Balasoorya, E.R., Jayasinghe, C.D., Jayawardena, U.A., Ruwanthika, R.W.D., Mendis de Silva, R., Udagama, P.V., 2017. Honey mediated green synthesis of nanoparticles: new era of safe nanotechnology. *Journal of Nanomaterials.*
- Chirumamilla, P., Vankudoth, S., Dharavath, S. B., Dasari, R., Taduri, S., 2022. In vitro anti-inflammatory activity of green synthesized silver nanoparticles and leaf methanolic extract of *Solanum khasianum* Clarke. *Proceedings of the National Academy of Sciences, India Section B: Biological Sciences.* 1-7.
- Choby, J., Howard-Anderson, J., Weiss, D., 2020. Hypervirulent *Klebsiella pneumoniae* clinical and molecular perspectives. *Journal of internal medicine.* 287 (3), 283–300.
- Chokshi, A., Sifri, Z., Cennimo, D., Horng, H., 2019. Global contributors to antibiotic resistance. *Journal of global infectious diseases.* 11 (1), 36.
- Das, R.P., Pradhan, A.K., 2022. An introduction to different methods of nanoparticles synthesis. *Bio-Nano Interface.*, 21–34
- David, A., Kumar, R., 2022. Biogenesis of MnO₂ nanoparticles using *Momordica Charantia* Leaf Extract. *ECS Transactions.* 107 (1), 747.
- Ghotekar, S., Pansambal, S., Bilal, M., Pingale, S.S., Oza, R., 2021. Environmentally friendly synthesis of Cr₂O₃ nanoparticles: characterization, applications and future perspective - A review. *Case Studies in Chemical and Environmental Engineering.* 3, 100089.
- Hao, G., Xiao, L., Hu, Y., Shao, F., Ke, X., Liu, J., Gao, H., 2019. Facile preparation of Cr₂O₃ nanoparticles and their use as an active catalyst on the thermal decomposition of ammonium perchlorate. *Journal of Energetic Materials.* 37 (3), 251–269.
- Hassan, D., Khalil, A.T., Solangi, A.R., El-Mallul, A., Shinwari, Z.K., Maaza, M., 2019. Physicochemical properties and novel biological applications of *Callistemon viminalis*-mediated α-Cr₂O₃ nanoparticles. *Applied Organometallic Chemistry.* 33 (8), e5041.
- Imraish, A., Abu Thiab, T., Al-Awaida, W., Al-Ameer, H.J., Bustanji, Y., Hammad, H., Al-Hunaiti, A., 2021. In vitro anti-inflammatory and antioxidant activities of ZnFe₂O₄ and CrFe₂O₄ nanoparticles synthesized using *Boswellia carteri* resin. *Journal of Food Biochemistry.* 45 (6), e13730.
- Iqbal, J., Abbasi, B.A., Munir, A., Uddin, S., Kanwal, S., Mahmood, T., 2020. Facile green synthesis approach for the production of chromium oxide nanoparticles and their different in vitro biological activities. *Microscopy research and technique.* 83 (6), 706–719.
- Kalaycıoğlu, Z., Geçim, B., Erim, F.B., 2022. Green synthesis of cerium oxide nanoparticles from turmeric and kinds of honey: characterisations, antioxidant and photocatalytic dye degradation activities. *Advances in Natural Sciences: Nanoscience and Nanotechnology.* 13, (1) 015016.
- Kamari, H.M., Al-Hada, N.M., Baqer, A.A., Shaari, A.H., Saion, E., 2019. Comprehensive study on morphological, structural and optical properties of Cr₂O₃ nanoparticle and its antibacterial activities. *Journal of Materials Science: Materials in Electronics.* 30 (8), 8035–8046.

- Khan, S.A., Shahid, S., Hanif, S., Almoallim, H.S., Alharbi, S.A., Sellami, H., 2021. Green synthesis of chromium oxide nanoparticles for antibacterial, antioxidant anticancer, and biocompatibility activities. *International Journal of Molecular Sciences*. 22 (2), 502.
- Kim, S. H., Yoo, S. H., Chakraborty, P., Jeong, J., Lim, J., El-Zoka, A. A., Neugebauer, J. r., 2022. Understanding alkali contamination in colloidal nanomaterials to unlock grain boundary impurity engineering. *Journal of the American Chemical Society*. 144 (2), 987-994.
- Kwak, G.Y., Han, Y., Baik, S., Kong, B.M., Yang, D.C., Kang, S.C., Sukweenadhi, J., 2022. Gold nanoparticles green-synthesized by the *Suaeda japonica* leaf extract and screening of anti-inflammatory activities on raw 267.4 macrophages. *Coatings*. 12 (4), 460.
- Lokapur, V., Jayakar, V., Divakar, M., Chalannavar, R.K., Lasrado, L., Shantaram, M., 2022. ZnO nanoparticles with spectroscopically controlled morphology, bioinspired from *Holigarna grahamii* (Wight) Kurz and delving its antioxidant and anticancer potential on A498 cell line. *Materials Today Communications*. 31, 103338.
- Lu, H., Zhang, X., Khan, S.A., Li, W., Wan, L., 2021. Biogenic synthesis of MnO₂ nanoparticles with leaf extract of *Viola betonicifolia* for enhanced antioxidant, antimicrobial, cytotoxic, and biocompatible applications. *Frontiers in Microbiology*. 12, 761084.
- Maheo, A.R., Vithiya, B.S.M., Prasad, T.A.A., Tamizhdurai, P., Mangesh, V., 2022. Biosynthesis, characterization, biological and photo catalytic investigations of *Elsholtzia blanda* and chitosan mediated copper oxide nanoparticles. *Arabian Journal of Chemistry*. 15, (3) 103661.
- Nivethitha, P. R., Rachel, D. C. J., 2020. A study of antioxidant and antibacterial activity using honey mediated chromium oxide nanoparticles and its characterization. *Materials Today: Proceedings*.
- Olga, M., Jana, M., Anna, M., Irena, K., Jan, M., Alena, Č., 2022. Antimicrobial properties and applications of metal nanoparticles biosynthesized by green methods. *Biotechnology Advances*. 107905.
- Pandiyani, I., Sri, S.D., Indiran, M.A., Rathinavelu, P.K., Prabakar, J., Rajeshkumar, S., 2022. Antioxidant, anti-inflammatory activity of *Thymus vulgaris*-mediated selenium nanoparticles: An in vitro study. *Journal of Conservative Dentistry: JCD*. 25 (3), 241.
- Patra, T., Mohanty, A., Singh, L., Muduli, S., Parhi, P.K., Sahoo, T. R., 2022. Effect of calcination temperature on morphology and phase transformation of MnO₂ nanoparticles: A step towards green synthesis for reactive dye adsorption. *Chemosphere*. 288, 132472.
- Perveen, S., Nadeem, R., ur Rehman, S., Afzal, N., Anjum, S., Noreen, S., Iqbal, M., 2022. Green synthesis of iron (Fe) nanoparticles using *Plumeria obtusa* extract as a reducing and stabilizing agent: Antimicrobial, antioxidant and biocompatibility studies. *Arabian Journal of Chemistry*. 15 (5), 103764.
- Rajakumar, G., Thiruvengadam, M., Mydhili, G., Gomathi, T., Chung, I.M., 2018. Green approach for synthesis of zinc oxide nanoparticles from *Andrographis paniculata* leaf extract and evaluation of their antioxidant, anti-diabetic, and anti-inflammatory activities. *Bioprocess and biosystems engineering*. 41 (1), 21–30.
- Rasouli, E., Basirun, W.J., Rezayi, M., Shameli, K., Nourmohammadi, E., Khandanlou, R., Sarkarizi, H.K., 2018. Ultrasmall superparamagnetic Fe₃O₄ nanoparticles: honey-based green and facile synthesis and in vitro viability assay. *International journal of nanomedicine*. 13, 6903.
- Riaz, T., Assey, N., Javed, M., Shahzadi, T., Zaib, M., Shahid, S., Alsaab, H.O., 2022. Biogenic plant mediated synthesis of monometallic zinc and bimetallic Copper/Zinc nanoparticles and their dye adsorption and antioxidant studies. *Inorganic Chemistry Communications*. 140, 109449.
- Ribeiro, A.I., Dias, A.M., Zille, A., 2022. Synergistic effects between metal nanoparticles and commercial antimicrobial agents: A Review. *ACS Applied Nano Materials*. 5 (3), 3030–3064.
- Russo, T.A., Marr, C.M., 2019. Hypervirulent *Klebsiella pneumoniae*. *Clinical microbiology reviews*. 32 (3), e00001–e19.
- Sabeena, G., Rajaduraiandian, S., Pushpalakshmi, E., Alhadlaq, H. A., Mohan, R., Annadurai, G., Ahamed, M., 2022. Green and chemical synthesis of CuO nanoparticles: A comparative study for several in vitro bioactivities and in vivo toxicity in zebra-fish embryos. *Journal of King Saud University. Science*. 102092.
- Sahli, C., Moya, S.E., Lomas, J.S., Gravier-Pelletier, C., Briandet, R., Hémadi, M., 2022. Recent advances in nanotechnology for eradicating bacterial biofilm. *Theranostics*. 12 (5), 2383.
- Sharma, U.R., Sharma, N., 2021. Green Synthesis, anti-cancer and corrosion inhibition activity of Cr₂O₃ nanoparticles. *Biointerf. Res. Appl. Chem*. 11, 8402–8412.
- Sone, B., Manikandan, E., Gurib-Fakim, A., Maaza, M., 2016. Single-phase α-Cr₂O₃ nanoparticles' green synthesis using *Callistemon viminalis* red flower extract. *Green Chemistry Letters and Reviews*. 9 (2), 85–90.
- Šuto, S., Bedenić, B., Likić, S., Kibel, S., Anušić, M., Tičić, V., Vraneš, J., 2022. Diffusion of OXA-48 carbapenemase among urinary isolates of *Klebsiella pneumoniae* in non-hospitalized elderly patients. *BMC microbiology*. 22 (1), 1–15.
- Tsegay, M., Gebretinsae, H., Nuru, Z., 2021. Structural and optical properties of green synthesized Cr₂O₃ nanoparticles. *Materials Today: Proceedings*. 36, 587–590.
- Vardakas, K.Z., Athanassaki, F., Pitiriga, V., Falagas, M.E., 2019. Clinical relevance of in vitro synergistic activity of antibiotics for multidrug-resistant gram-negative infections: A systematic review. *Journal of Global Antimicrobial Resistance*. 17, 250–259.
- Velsankar, K., Venkatesan, A., Muthumari, P., Suganya, S., Mohandoss, S., Sudhahar, S., 2022. Green inspired synthesis of ZnO nanoparticles and its characterizations with biofilm, antioxidant, anti-inflammatory, and anti-diabetic activities. *Journal of Molecular Structure*. 1255, 132420.
- Vernekar, N.S., Taranath, T.C., 2022. Sunlight-assisted fabrication of silver nanoparticles using *Terminalia neotaliala* Capuron Aqueous Bark Extract: Evaluation of in vitro antioxidant and anti-inflammatory activities. *Nanomedicine Research Journal*. 7 (3), 235–244.
- Wang, L., Hu, C., Shao, L., 2017. The antimicrobial activity of nanoparticles: present situation and prospects for the future. *International journal of nanomedicine*. 12, 1227.
- Wang, C., Karmakar, B., Awwad, N.S., Ibrahim, H.A., El-kott, A. F., Abdel-Daim, M.M., Batiha, G.E.S., 2022. Bio-supported of Cu nanoparticles on the surface of Fe₃O₄ magnetic nanoparticles mediated by *Hibiscus sabdariffa* extract: Evaluation of its catalytic activity for synthesis of pyrano [3, 2-c] chromenes and study of its anti-colon cancer properties. *Arabian Journal of Chemistry*. 15, (6) 103809.
- Yassin, M.T., Mostafa, A.A.F., Al-Askar, A.A., Al-Otibi, F.O., 2022. Facile green synthesis of silver nanoparticles using aqueous leaf extract of *Origanum majorana* with potential bioactivity against multidrug resistant bacterial strains. *Crystals*. 12 (5), 603.